CENATAV
Centro de Aplicaciones de
Tecnologías de Avanzada
MINISTERIO DE LA INDUSTRIA BÁSICA

RNPS No. 2142
ISSN 2072-6287
Versión Digital

REPORTE TÉCNICO

Reconocimiento de Patrones

SERIE AZUL

High Resolution Palmprint Matching: A Review

Manuel Aguado Martínez and
José Hernández Palancar

RT_069 **febrero 2015**

7ma. No. 21812 e/218 y 222,
Rpto. Siboney, Playa;
La Habana.
Cuba. C.P. 12200
www.cenatav.co.cu

CENATAV
Centro de Aplicaciones de
Tecnologías de Avanzada
MINISTERIO DE LA INDUSTRIA BÁSICA

RNPS No. 2142
ISSN 2072-6287
Versión Digital

SERIE AZUL

REPORTE TÉCNICO
Reconocimiento de Patrones

High Resolution Palmprint Matching: A Review

**Manuel Aguado Martínez and
José Hernández-Palancar**

RT_069 **febrero 2015**

7ma. No. 21812 e/218 y 222,
Rpto. Siboney, Playa;
La Habana.
Cuba. C.P. 12200
www.cenatav.co.cu

Table of Content

List of Figures

List of Tables

High Resolution Palmprint Matching: A Review

Manuel Aguado Martínez and José Hernández Palancar

Biometrics Research Team, Advanced Technologies Application Center (CENATAV),
Havana, Cuba
{maguado, jpalancar}@cenatav.co.cu

RT_069, Serie Azul, CENATAV
Aceptado: 8 de enero de 2015

Abstract. The study of palmprint has become in recent years a very important biometric field since its wide use in forensic applications, as well as, in access control and authentication applications. In forensic applications, for example, palmprint have a huge impact since they appear frequently in crime scenes and in some cases are the only kind of latent impression found. Statistical studies show that 30% of the latent prints recovered from crime scenes are from palms. The research field of palmprint can be divided in two categories: online palmprint matching and offline palmprint matching. Online palmprint matching uses low resolution images (150 dpi or less) and offline palmprint matching uses high resolution images (500 dpi or more). In this work, a new taxonomy of the principal palmprint matching techniques reported in the literature corresponding to the last category is presented, as well as, the remaining unsolved problems detected and some possible research lines to be study in the future.

Keywords: palmprint, high resolution palmprint matching, latent palmprint matching, partial palmprint matching, orientation field estimation in palmprints.

Resumen. Las impresiones palmares han cobrado en los últimos años una gran importancia en la biometría debido a su amplio uso tanto en las aplicaciones forenses como en las aplicaciones de control de acceso y autenticación. En las aplicaciones forenses por ejemplo, las impresiones palmares aparecen frecuentemente en escenas del crimen, siendo en algunos casos el único tipo de huella latente encontrado. Estudios estadísticos corroboran lo anterior mostrando que el 30% de las impresiones latentes en escenas del crimen corresponden a palmares. El campo de investigación de las impresiones palmares puede ser dividido en dos categorías: cotejo online de impresiones palmares y cotejo offline de impresiones palmares. En el cotejo online de impresiones palmares se utilizan imágenes de baja resolución (150 dpi o menos) mientras que en el cotejo offline de impresiones palmares se utilizan imágenes de alta resolución (500 dpi o más). En este trabajo se presentará una nueva taxonomía de las principales técnicas de cotejos de palmares en la última categoría, así como, los principales problemas detectados que permanecen sin ser solucionados y algunas posibles líneas de investigación a ser abordadas en el futuro.

Palabras clave: impresiones palmares, cotejo de impresiones palmares con alta resolución, cotejo de impresiones palmares latentes, cotejo de impresiones palmares parciales, estimación del campo de orientación en impresiones palmares.

1 Introduction

The study of palmprint has become in recent years a very important biometric field since its wide use in forensic applications, as well as, in access control and authentication applications. Although fingerprint is the most widely used biometric trait, where some small features called minutiae are used to compare one fingerprint to another, it is problematic to detect the minutiae from fingers of elderly people and manual workers [1]. The main advantage of palmprint is the large area of the palm that contains rich and useful information which makes it highly individual [2].

The palm is the inner region of the hand excluding the fingers. Palmprint is referred to skin's pattern of the surface of the palm. The pattern of the skin on the palm is formed by the combination of ridges and creases. Creases are classified as principal lines, minor creases and secondary creases [3], secondary creases are also called wrinkles and they are much thinner and irregular than the others. principal lines are known as the lines of the head, life and heart (See Figure 1), they are stable features given they vary little over time [3]. Based on the principal lines, the palm is divided in three regions: interdigital, hypothenar eminence and thenar eminence. Generally the thenar eminence has the biggest concentration of secondary creases (See Figure 1).

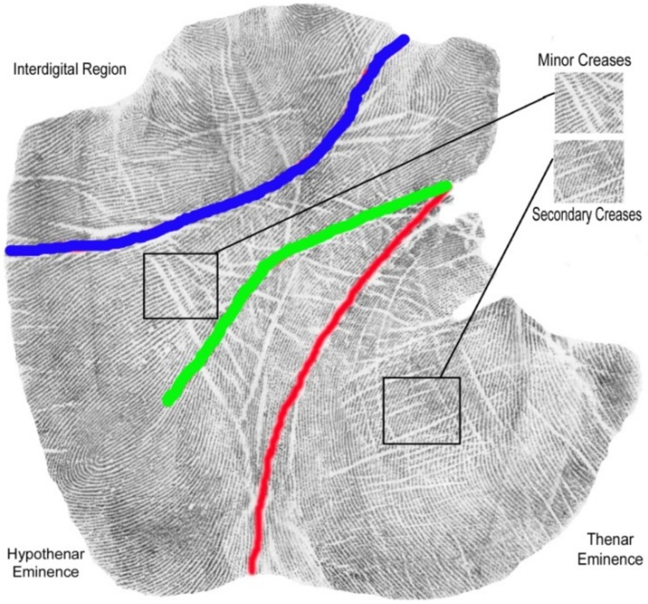

Fig. 1. Palmar Regions (Interdigital, Hypothenar Eminence, Thenar Eminence). Major creases: the heart line (blue), the head line (green), and the life line (red). Minor and secondary creases.

The minutiae are formed by terminations and bifurcations of ridges, so they could be extracted as a distinctive feature (See Figure 2), there are other types of minutia but these are the most widely used. Other features that can be extracted from palmprints are orientation field and density map, defined as the ridges orientation and ridge density in different local regions respectively. Additional features that could be simultaneously obtained from a palmprint can be found in [4].

The research field of palmprint can be divided in two categories: online palmprint matching and offline palmprint matching (See Figure 3). Online palmprint matching uses low resolution images (150 dpi or less) and offline palmprint matching uses high resolution images (500 dpi or more). Features like ridges, singular points and minutiae do not appear in low resolution images, while principal lines, wrinkles and texture are still present. High resolution images are usually used in forensic applications while low resolution images are used in civil and commercial applications due to their smaller size and short processing time.

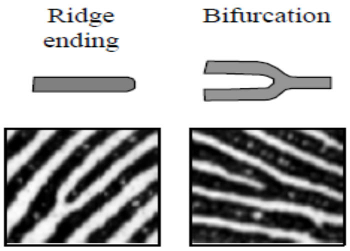

Fig. 2. Two types of minutia [5].

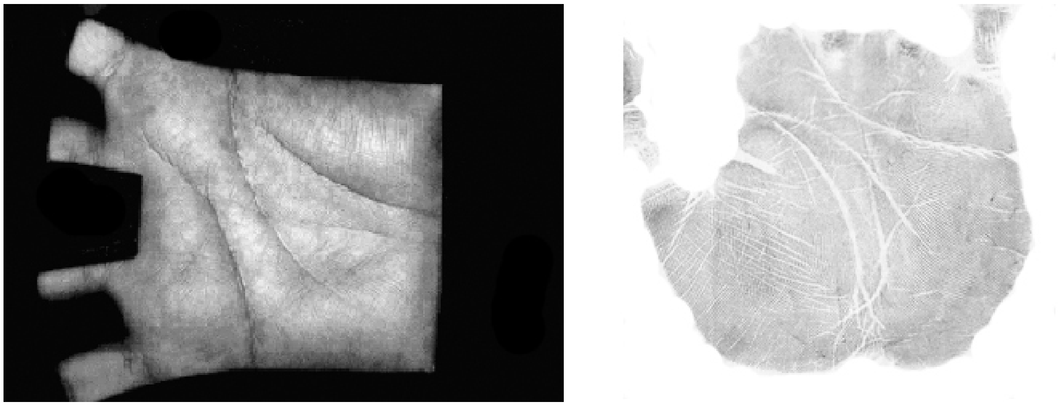

Fig. 3. Images of low resolution (online palmprint matching) and high resolution (offline palmprint matching).

The major techniques developed in high resolution palmprint matching are discussed in this article. In section 2 of this paper, some algorithms proposed in the literature to reliably extract the minutiae information avoiding the negative effects provoked by creases are discussed. In section 3, the palmprint matching techniques that only use the information relative to the minutiae position and direction are presented, while in section 4, multi-features high resolution palmprint matching techniques are covered. The previous two sections will be covering partial-to-full and latent-to-full matching approaches, section 5 will be covering full-to-full palmprint matching systems. Finally, in section 6 some conclusions are presented. In the next subsection, some particularities of the offline palmprint matching are introduced. Figure 4 illustrates the proposed taxonomy.

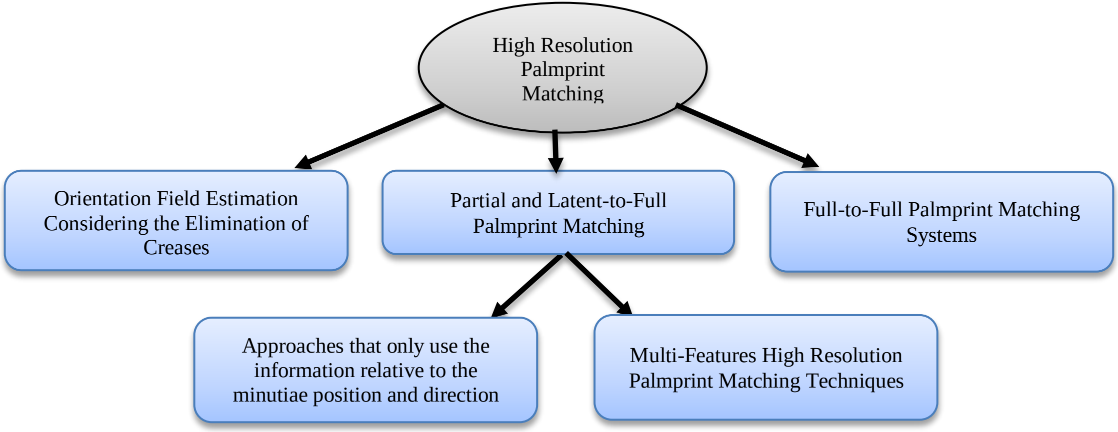

Fig. 4. Proposed taxonomy of the principal high resolution palmprint matching techniques.

1.1 High Resolution (Offline) Palmprint Matching

As was mentioned above, offline palmprint matching uses high resolution images (500 dpi or more) and its scope is mainly the forensic field. The importance of palmprint in this field is corroborated by statistics studies that show that 30% of the latent prints recovered from crime scenes are from palms [6]. Therefore, latent-to-full palmprint matching algorithms are one of the biggest interests of law agencies. Latent-to-full palmprint matching is a challenging task due to the problems associated with the latent impressions. Latent impressions (See Figure 5) are only a small part of the palmprint and generally have poor quality and noise associated to the background surface which causes the detection of spurious minutiae. Furthermore latent impressions often do not contain any singular or reference point that can be used for the alignment. Full-to-full and partial-to-full system are used in access control and borders.

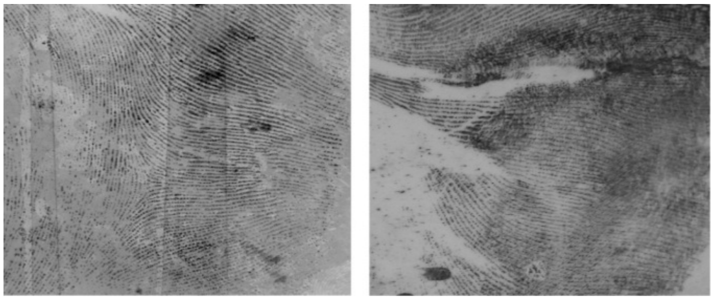

Fig. 5. Two Latent Impressions.

Although some algorithms for fingerprint matching could be used for palmprint matching many authors pointed a number of differences between palmprints and fingerprints that make those algorithms are unsuitable for the palmprint matching task [7, 8]. The principal differences cited are:

- High density of creases: Although fingerprints could have some creases, generally these creases are very thin and their number is small. As we saw in the introduction, palmprints have a wide number of creases with variable width. Also generally the thenar region has a high density of creases which makes difficult the estimation of the ridge orientation field and therefore causes the detection of many spurious minutiae.
- Palmprint Size: Since the palmprint area is much bigger than fingerprint area, the sizes of palmprint images are also bigger than the sizes of fingerprint images, which causes an increase in the preprocessing and post processing time of a palmprint image. This also leads to a major number of minutiae, so the matching process is computationally more expensive. For example, in [8] the authors pointed that VeriFinger [9], an awarded commercial matcher, can perform more than 15000 fingerprint matches per second but only three palmprint matches per second.
- Skin distortion: The non-linear distortion between two prints of the same palm is often very big due to the palmprint size and its physical structure [8]. Figure 6 shows two prints of the same palm with big non-linear distortion. In [8] the authors show how the skin distortion is widely present in palmprints principally in the thenar region.
- Absence of the central region: In most of the latent palmprints and in those captured by a contact-based device the central region of the palm is missing. This is also due to the physical structure of the palmprints. Although there is still plenty information available, this causes that the principal lines are not a very robust feature. Figure 7 shows two palmprints with the central region missing.
- Difference of quality and discriminative power of the palmprints features between regions: As we previously mentioned the thenar eminence has the biggest concentration of creases therefore this region has poorer quality than the others. In [8] the authors run a study about the discriminative power of the principal palmprint features (minutiae, orientation field, density map) in different regions of the palm, found that the features have different discriminative power between regions.

Figure 8 was taken from [8] and shows the different discriminative power of the features studied between regions. The minutiae have the lowest discriminative power around the thenar region; this is caused by the high density of creases of this region which affects as we later show the minutiae extraction and the high nonlinear distortion of this region. This study also shows that the density map is a discriminative feature for palmprint recognition and also that it has consistent discriminative power between regions. Furthermore, in [10] the authors also run some tests by matching different regions manually segmented with MegaMatcher 4.0 SDK [11] obtaining EERs of 0.89%, 1.18% and 6.57% for hypothenar, interdigital and thenar regions respectively.

Therefore, the algorithms designed for palmprint must take into account the above differences and also exploit the intrinsic characteristics of palmprints. For example, in [10] the authors propose the use of logistic regression to fusion the different regions scores obtaining an EER of 0.25% compared to 1% of full-to-full comparison.

Fig. 6. Two prints of the same palm with big non-linear distortion caused by different pressures. The squares show an example of an area with non-linear distortion between the prints.

Fig. 7. Two palmprints with the central region missing.

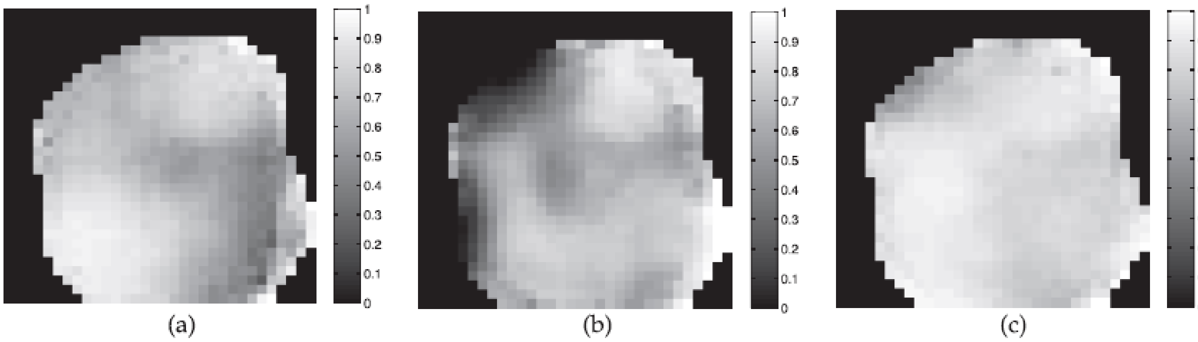

Fig. 8. Different discriminative power of different features between different regions: a) minutiae, b) orientation field, c) density map. The brighter regions are the regions with most discriminative power by feature [8].

2 Ridges Extraction Algorithms

Because the minutiae are formed by the bifurcations and terminations of ridges, the extraction of ridges is a crucial step on the minutiae detection algorithms. As we previously mentioned, the presence of a large number of creases in palmprints makes difficult the estimation of the ridge orientation field. There is a wide number of algorithms to estimate the orientation field in fingerprints that can be classified in three groups [5]:

- Gradient based approaches: These approaches are under the premise that the gradient phase angle denotes the maximum intensity change and therefore the direction of a ridge is orthogonal to the gradient phase angle [5], but this is not quite true in areas with high density of creases because the creases can behave like ridges and therefore it is quite difficult to distinguish between them based only in a directional criterion.
- Slit and projection based approaches: These approaches are based on the method proposed in [12]. The basic idea is that, the sum of the gray values is small for pixels belonging to ridges and high for pixels belonging to valleys. But in palmprints for pixels belonging to creases, the sum of the gray values is also high. Also, since creases and ridges cross each other, the sum of the gray values of pixels belonging to ridges is not too small, and in areas with high density of creases this value tends to be high also.

  Orientation estimation in the frequency domain: These methods assume that except for singular points any local region has a consistent orientation and frequency, and therefore the spectrum in the frequency domain has two peaks that indicate the two parallel ridges that cross over the region, but once again this is not quite true in a local region of a palmprint with high density of creases because the creases cause the detection of multiple peaks.

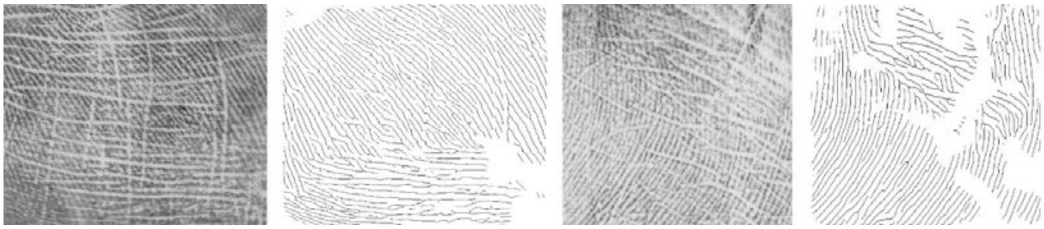

Fig. 9. The ridge skeleton produced by VeriFinger 4.2 in a palmar region with many creases.

The global model based methods for the regularization of the fingerprint orientation have also some problems when they are applied to palmprints based principally in that the ridge pattern in palmprints has no global consistency. Another way of saying this is that in palmprints different areas of an image have different patterns.

Figure 9 shows how VeriFinger, one of the most successful fingerprint recognition software [9], fails in estimating the ridge orientation field in a palmar area with high density of creases.

To overcome the above problems, in [13] a method that considers the elimination of creases was proposed as a way to provide a more robust estimate of the orientation field. The basic idea is to select a group of ridge candidates from a local image by fitting it to a ridge model. Then the correct candidates are selected on the basis of their continuity with the neighbor candidates which most likely are ridges according to the model. The proposed model to fit to the local image is a 2-dimensional sine wave.

Since a pair of parallel ridges crossing over a local image corresponds to two peaks in its power spectrum, the local image is fit to the model by detecting such peaks. As some peaks also represent creases, more than two peaks are detected for each local image to obtain a group of candidates. The peaks are detected in order of their amplitude. Figure 10 shows how not always the strongest sine wave represents the ridges of a local image.

For each small local area of $M \times M$ pixels a local region $h^{I_{i,j}}(x,y)$ of $L \times L$ pixels (L >M) is defined as:

$$g^{I_{i,j}}(x,y) = \left(-\frac{L}{2}+1 \le x,y \le \frac{L}{2}\right), \tag{1}$$

$$dc^{I_{i,j}} = \sum_{x=-\frac{L}{2}+1}^{L/2} \sum_{y=-\frac{L}{2}+1}^{L/2} w(x,y) g^{I_{i,j}}(x,y), \tag{2}$$

$$h^{I_{i,j}}(x,y) = w(x,y)\left(g^{I_{i,j}} - dc^{I_{i,j}}\right), \tag{3}$$

where $w(x,y)$ is a window Gaussian function. The power spectrum of $h^{I_{i,j}}(x,y)$ is denoted as $H^{I_{i,j}}(x,y)$, the K peaks are detected in $\left|H^{I_{i,j}}(x,y)\right|^2$.

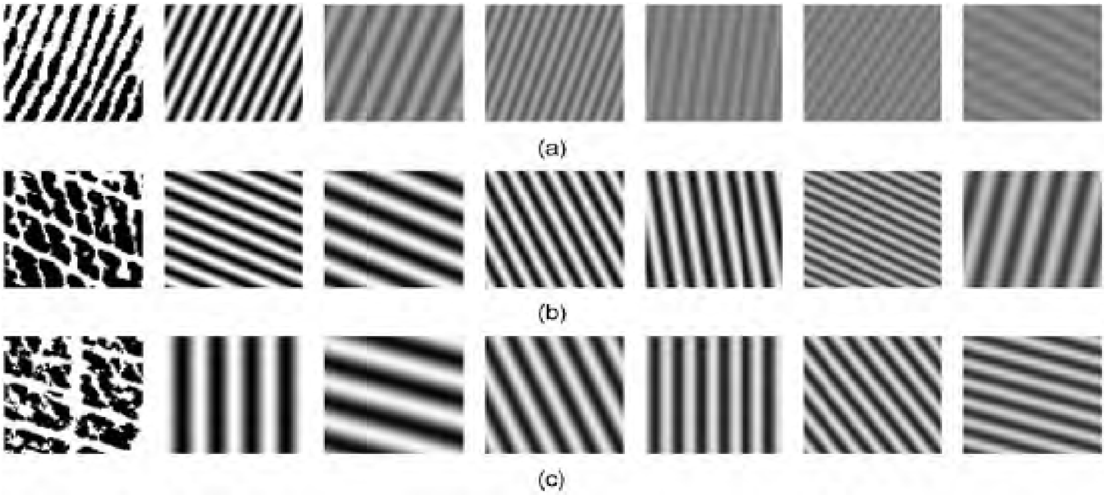

Fig. 10. The first six sine waves taken by their amplitudes in a local palmar image. In (b) and (c) the ridges are represented by the third sine wave [7].

The parameters of a peak located at the position (x_H, y_H) are calculated as follows:

$$a = 2\left|H^{I_{i,j}}(x_H, y_H)\right| , \tag{4}$$

$$ph = \tan^{-1}\frac{Im\left(H^{I_{i,j}}(x_H, y_H)\right)}{Re\left(H^{I_{i,j}}(x_H, y_H)\right)}, \tag{5}$$

$$d = \tan^{-1}\frac{x_H}{y_H}, \tag{6}$$

$$f = \frac{\sqrt{(x_H)^2 + (y_H)^2}}{L}, \tag{7}$$

$$e = \frac{4\pi^2\sigma^4}{L^2}\sum_{(x'_H, y'_H)\in V} 2\left|H^{I_{i,j}}(x'_H, y'_H)\right|^2, \tag{8}$$

where a, ph, d, f and e are the amplitude, phase, direction, frequency and energy respectively, σ is the variance of the Gaussian function $w(x, y)$ and V is the set of the 8-neighbor pixels to (x_H, y_H). The local region expressed by a, ph, d and f is:

$$G(x, y) = a\cos\big(f(x\cos d + y\sin d)\big) - ph\,. \tag{9}$$

The next step is the detection of which candidates in some local areas are most likely ridges. Such candidates are called “high reliability candidates” and those areas “high reliability areas”. Then, those candidates in the other areas having high continuity with the high reliability candidates are selected as ridges as well. First, all the first candidates of each local area are marked as ridges; the authors argue that the first candidate has the highest likelihood of being a ridge according to local information alone. This is true only in those local areas that do not have creases. Since as they pointed, the local information of the ridges generally does not have continuity with that of creases, groups of local areas are detected based on the continuity of the local information of its first candidates. Figure 11 shows a block diagram of the candidate selection process.

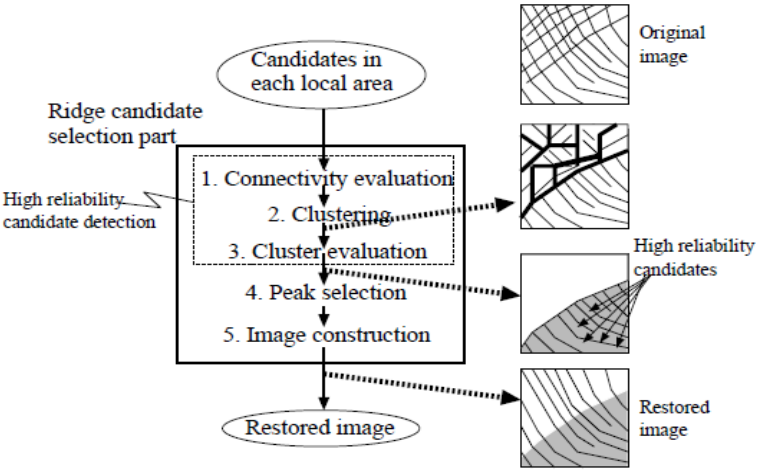

Fig. 11. Candidate selection process [13].

The connectivity or continuity of the local information of the first candidates in two adjacent areas is evaluated using the following features:

$$J_{dir} = \left| \left(\left| d_1^{I_{i,j}} - d_1^{I_{neighbor}} \right| + \frac{\pi}{2} \right) \, mod \, \pi - \frac{\pi}{2} \right| , \tag{10}$$

$$J_{pitch} = \left| \frac{1}{f_1^{I_{i,j}}} - \frac{1}{f_1^{I_{neighbor}}} \right| , \tag{11}$$

$$J_{ph} = \left| \left(ph_1^{I_{i,j}} - t\left(ph_1^{I_{neighbor}} \right) + \pi \right) \, mod \, 2\pi - \pi \right| , \tag{12}$$

here J_{dir}, J_{pitch} and J_{ph} are the difference in the direction, the pitch and the phase respectively, $t\left(ph_1^{I_{neighbor}}\right)$ is the translation formula to the coordinate system of $ph_1^{I_{i,j}}$ and is defined as:

$$t_{i,j}\left(ph_n^{I_{i+1,j}}\right) = \left(ph_n^{I_{i+1,j}} - 2\pi M f_n^{I_{i+1,j}} \cos d_n^{I_{i+1,j}} + \pi\right) mod \, 2\pi - \pi \, , \tag{13}$$

$$t_{i,j}\left(ph_n^{I_{i,j+1}}\right) = \left(ph_n^{I_{i,j+1}} - 2\pi M f_n^{I_{i,j+1}} \sin d_n^{I_{i,j+1}} + \pi\right) mod \, 2\pi - \pi \, . \tag{14}$$

When J_{dir}, J_{pitch} and J_{ph} are below of three predefined thresholds the candidates are considered connected. Now the connected candidates are clustered and those clusters are evaluated to be classified as high reliability areas. The features used to evaluate the clusters are:

1. The number of local areas included in a local area group (N_l).
2. The ratio of the energy of all the first candidates to the total energy of the local areas included in the clusters:

$$R_{cl} = \frac{\sum_{(i,j)\in C_l} e_1^{I_{i,j}}}{\sum_{(i,j)\in C_l} e_t^{I_{i,j}}} , \tag{15}$$

$$e_t^{I_{i,j}} = \frac{4\pi^2\sigma^4}{L^2} \sum_{x_H=-\frac{L}{2}+1}^{L/2} \; \sum_{y_H=-\frac{L}{2}+1}^{L/2} \left| H^{I_{i,j}}(x_H, y_H) \right| ,^2 \tag{16}$$

where C_l is the l-th cluster. Clusters with $N_l = \max(N)$ or with N_l and R_{cl} bigger than two predefined thresholds are classified as high reliability clusters and therefore their first candidates are classified as ridges. To use these features the authors argued that because of connectivity, the size of clusters in areas without creases is bigger than in those areas with high density of creases. This might have some problems in palmprints with high density of creases in the whole image and very poor quality, as is the case of the latent palmprints, because the ridge areas do not tend to grow much and in palmprint areas with large and strong creases the creases region might grow too much and be classified therefore as a ridge region. Figure 12 shows examples of those cases.

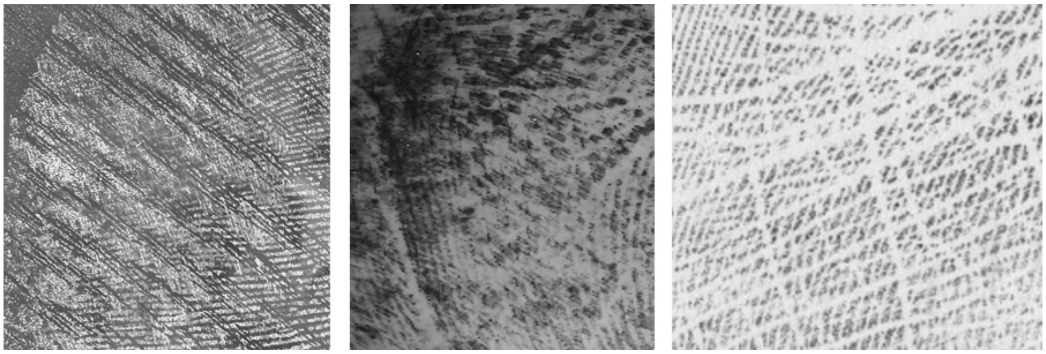

Fig. 12. Two latent palmprints with high density of creases and poor quality and one palmprint area with large and strong creases.

The final step is to select which of the candidates in clusters that were not selected as high reliability clusters are ridges, based on the connectivity with those in high reliability clusters. To do this a region growing algorithm is applied using the following features:

1. The ratio of the energy of a candidate to the energy of the others:

$$R_k^{I_{i,j}} = \frac{e_k^{I_{i,j}}}{\sum_{n=1}^{K} e_n^{I_{i,j}}}, \tag{17}$$

where K is the number of selected peaks.

2. The order of candidate k.
3. Average difference of the candidate phase:

$$D_{ph_k}^{I_{i,j}} = \frac{1}{\left\|U_N^{I_{i,j}}\right\|} \sum_{u^{I_{i',j'}} \in U_N^{I_{i,j}}} \left| \left(t_{i,j}\left(ph^{I_{i',j'}}_{u^{I_{i',j'}}} \right) - ph_k^{I_{i,j}} + \pi \right) mod\ 2\pi - \pi \right|, \tag{18}$$

where $U_N^{I_{i,j}}$ is a set of definite candidates in the adjacent areas to $I_{i,j}$.

4. Average difference of the candidate direction:

$$D_k^{I_{i,j}} = \frac{1}{\left\|U_S^{I_{i,j}}\right\|} \sum_{u^{I_{i',j'}} \in U_S^{I_{i,j}}} \left| \left(\left| d^{I_{i',j'}}_{u^{I_{i',j'}}} - d_k^{I_{i,j}} \right| + \frac{\pi}{2} \right) mod\ \pi - \frac{\pi}{2} \right|, \tag{19}$$

where $U_S^{I_{i,j}}$ is a set of definite candidates in the areas which satisfy $(i - i')^2 + (j - j')^2 \leq S$. The definite candidate with the minimum value of $D_k^{I_{i,j}}$ is selected from those candidates that satisfy $D_{ph_k}^{I_{i,j}} < TH_{ph},\ k < TH_K\ and\ R_k^{I_{i,j}} > TH_r$. Here TH_{ph}, TH_K and TH_r are predefined thresholds.

In [7] Jain et al. mention two drawbacks of the above procedure:

1. Crease regions may be incorrectly classified as ridge regions and are grown in the region growing procedure.
2. The enhanced image is not smooth due to the blocking effect which produces spurious minutiae.

Two main modifications are proposed to overcome the above drawbacks:

1. The selected regions are grown in the seed stage (high reliability clusters) separately and then one region is selected as a ridge region and merged with those compatible with it.

2. To solve the blocking effect problem, the ridge direction and frequency obtained are smoothed and Gabor filters are used to enhance the palmprint image.

There are some stages in the procedure described in [7] that slightly differs from their equivalent in [13]. Those differences are:

1. The DC component is not subtracted to the local image before multiplying it by the Gaussian window function.
2. To determine if two waves are continuous, instead of using the phase difference of the two waves, the authors use the difference of their normalized gray-scale value:

$$D_{gs} = \frac{1}{16} \sum_{x=-\frac{L}{2}+1}^{L/2} \sum_{y=-\frac{L}{2}+1}^{L/2} \left| \frac{G_1(x,y)}{a_1} - \frac{G_2(x,y)}{a_2} \right| . \qquad (20)$$

3. To form the groups of connected first waves they do not use all the first candidates, instead of this the reliability of the first candidates is calculated as $a_1/(a_1+a_2)$ where a_1 y a_2 are the first and the second candidate. Those candidates with reliability bigger than a predefined threshold are selected to form the groups. As was previously mentioned, the groups are no classified as crease regions and ridge regions.
4. For the region growing algorithm, only the groups with cardinality bigger than a predefined threshold are used as seeds instead of using all of them. Those seeds are organized in descending order according to their size. Each seed is then grown by turn and separately from the others, this means that for each iteration they assume that there is only one seed.
5. In the region growing algorithm those candidate waves that are continuous with the adjacent candidates in the current region are selected iteratively. If a candidate selected is a first candidate and also belongs to a seed not analyzed yet, then that seed is invalidated but previously merged with the current region. After this process they have obtained a set of regions.
6. The regions obtained are sorted in decreasing order according to the number of reliable first waves. The first region is selected as a ridge region and copied to the final region. The other regions with no overlapped blocks with the final region are also copied to the final region. Those regions with overlapped blocks are copied to the final region only if the selected waves in the overlapped blocks are the same.

   Although the experiments show that with this procedure performs better than the procedure described in [13], the authors claim that there are still some problems in noisy high curvature areas. We can also note the following drawbacks associated to the region growing procedure:

1. If the region with the most reliable first waves was obtained from a crease seed, then the procedure fails in detecting the ridge region.
2. If a region obtained from a crease seed has no overlapped blocks with the ridge regions, then this region is copied to the final region and therefore the final region contains creases.

Despite the fact that the above algorithms can identify ridges in region with creases, both of them still have some problems in regions with high density of creases. In [14] a new method to reliably estimate the initial orientation field even in regions with high density of creases was presented based on the Radon transform. The reason behind the use of the Radon transform is that the ridge direction is slowly-varying in a local area and therefore it can be approximated by a straight line. The problems with this method is that it is computational expensive so they propose to first detect the creases and then, in those areas with low density of creases apply the algorithm proposed in [7] and in the areas with high density of creases apply the algorithm based on the Radon transform. Finally, both areas are merged by using the region growing algorithm proposed in [7]. The Figure 13 taken from [14] shows that the radon transform works better in a region with more creases than the procedure based on the DFT described in [7].

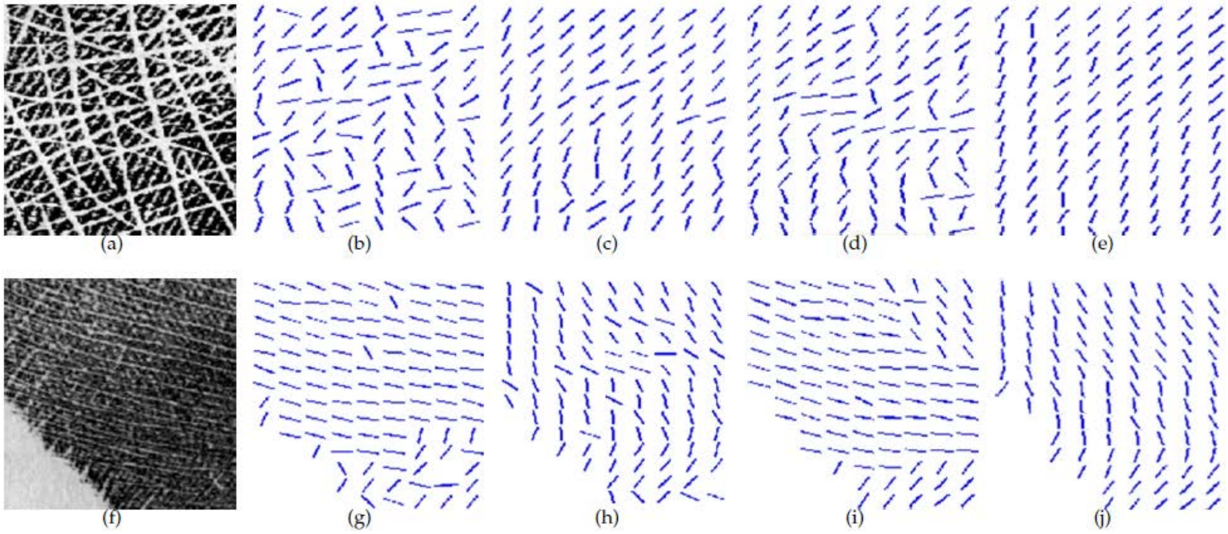

Fig. 13. Comparison between the method based on the DFT described in [7] and the procedure described in [14] based on the Radon transform in regions with high density of creases: (a) and (f) are the original images, (b) and (g) are the initial orientation fields estimated by [7], (c) and (h) are the initial orientation fields estimated by [14], (d) and (i) are the final orientation fields estimated by [7], (e) and (j) are the final orientation fields estimated by [14]. This figure was taken from [14].

Firstly the image is divided in blocks of 16X16 and the algorithm proposed in [15] is utilized to extract creases from this blocks. The quality value for each block is computed as the sum of the crease energy values for all the creases present inside a 64X64 pixel neighboring region. The DFT method proposed in [7] is applied for the neighboring region whose crease energy is smaller than a threshold. At this point for each selected peak (u_i, v_i) the direction (phase) and the ridge density (frequency) are computed. To compute the direction they apply the next formula that differ from the formula described in [7]:

$$\theta_i = \tan^{-1}\left(\frac{u_i}{v_i}\right) - \frac{\pi}{2} \ . \tag{21}$$

The formula to compute the ridge density is the same as in [7]. For the neighboring regions whose crease energy is bigger than certain threshold, a method based on the Radon transform is proposed. Since the original Radon transform is performed at the whole image and they just want to apply it on a small local area, they utilize the modified finite Radon transform described in [15].

First, all the pixels in the neighboring area are scanned, and those whose grayscales are smaller than a threshold are selected. For each pixel (x_i, y_i) selected a normalization is performed in a circular region Δ of radius 27 and centered at (x_i, y_i) by subtracting the mean of the grey levels from every pixel. Next the modified finite Radon transform is applied as:

$$r(\theta; x_i, y_i) = \sum_{(x,y)\epsilon\Delta} I(x,y)'\delta((x - x_i)\cos\theta + (y - y_i)\sin\theta)\ , \tag{22}$$

where $I(x,y)'$ is the normalized grey level at pixel (x,y) and θ is the direction of the line. Let θ_0 the direction that minimizes $r(\theta; x_i, y_i)$, then a confidence value is associated to the estimated value given by:

(23)

$$c_i(x_i, y_i) = -\,r(\theta_0; x_i, y_i)\,.$$

Since all the points with the same direction in the neighboring area ∇ should be taken into consideration, the aggregate confidence value of each direction is computed as:

$$c_b(\varphi) = \sum_{(x,y)\in\nabla} f(c_0(x,y))I(\theta_0(x,y) = \varphi)\,, \tag{24}$$

$$f(c) = \begin{cases} 0 & if\ c \le c_T \\ c & if\ c > c_T \end{cases}\,, \tag{25}$$

where c_T is the truncation threshold that was empirically set as 200 in their experiments. After this, the algorithm described in [16] is applied to extract the ridge density along each one of the k directions with the top confidence values. Finally the region growing algorithm described in [7] is used to select the final orientation. Two ridges (θ_a, f_a) and (θ_b, f_b) are continuous if they meet the following conditions:

$$\begin{cases} |\theta_a - \theta_b| \le \dfrac{\pi}{6} \\ \left|\dfrac{1}{f_a} - \dfrac{1}{f_b}\right| \le 3 \end{cases}\,. \tag{26}$$

Even though the authors obtained better results with this method than the other one, the same drawbacks associated to the region growing algorithm in [7] are still present. Furthermore another concern with this method in palmprints with high density of creases (i.e. palmprints from elderly people and manual workers or latent impressions from the thenar region), is the high computational cost of the Radon transform.

In conclusion ridge extraction in palmprints is a very important problem that has not be completely solved yet. The algorithms of the state of the art present some major drawbacks related mainly to the presence of many and wide creases and to the region growing algorithm used as a post smooth algorithm. One way to address these issues is by a better and robust selection of the ridge candidates in each local area. Thus a much deeper study is needed in this area to overcome the above problems.

3 Partial Palmprint Matching Methods Based Only on Minutiae Position Information

The methods based only on Minutiae Position Information (coordinates and direction) are very important since as was previously pointed, the latent palmprint images are of poor quality and therefore in many cases the features extraction from those is performed manually by forensic experts. Another reason is that the other types of features are not currently standardized, so they have limited use in a global and interoperable biometric system.

The method described in [17] computes the local matching based on the local structure of the minutiae and the global similarities between two minutiae sets, then both scores are combined to obtain a final similarity measure between the two palmprints.

To construct the local structure of each minutia $p(x, y, \theta)$ $(x, y$ are the abscissa and the ordinate of the minutiae and θ is the direction of the minutiae) a local polar coordinate system is built by setting as the origin and the axis direction the position and the direction of the minutiae respectively. The authors argue that the use of the polar coordinate system could describe the nonlinear distortion better, and it is easier to handle the translation and rotation of the image. Then a local eigenvector of length $3(n+1)$ is constructed with the n-nearest neighborhood minutiae according to their polar radius to the origin. The eigenvector is defined as:

$$(x, y, \theta, r_1, \varphi_1, \alpha_1, r_2, \varphi_2, \alpha_2, \ldots, r_n, \varphi_n, \alpha_n)\,, \tag{27}$$

$$r_i = \sqrt{(x_i - x)^2 + (y_i - y)^2}\,, \tag{28}$$

$$\varphi_i = \tan^{-1}\left(\frac{y_i - y}{x_i - x}\right), \tag{29}$$

$$\alpha_i = \theta_i - \theta\,, \tag{30}$$

where r_i is the polar radius, φ_i is the polar angle and α_i is the relative direction that is to say the difference of the directions. The neighborhood minutiae are sorted in ascending order according to the polar radius. The direction of a minutia is defined as the angle between the tangent to the ridge line at the minutia position and the horizontal axis (Figure 14).

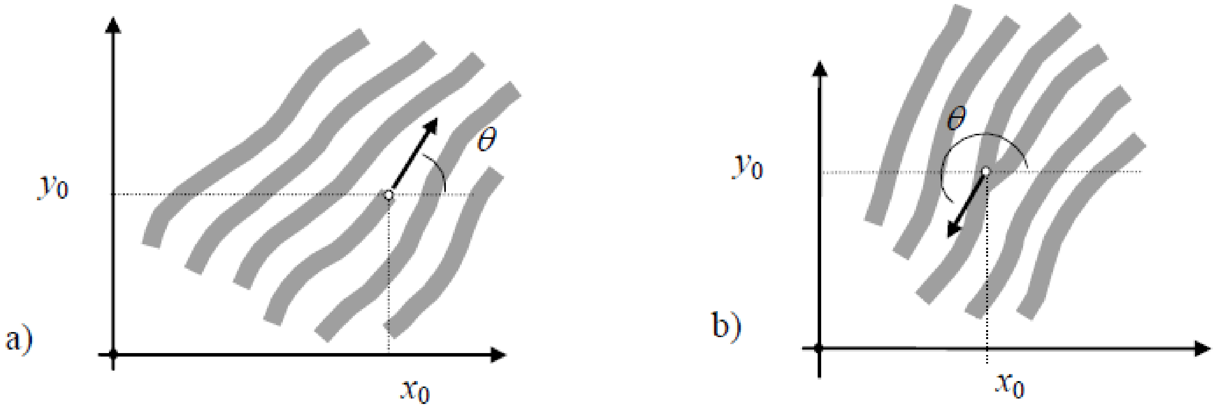

Fig. 14. The directions of a ridge ending minutia (a) and a bifurcation minutia (b) [5].

The matching score between two local structures is the number of matching minutiae in its neighborhood. Two minutiae *i* and *j* match each other if the following conditions are met:

$$|r_i - r_j| < \delta_1\,, \tag{31}$$

$$|\varphi_i - \varphi_j| < \varepsilon_1\,, \tag{32}$$

$$|\alpha_i - \alpha_j| < \gamma_1\,. \tag{33}$$

The matching extent of the two neighbor minutiae is defined as:

$$M_l(i,j) = |r_i - r_j| + \mu_1|\varphi_i - \varphi_j| + \mu_2|\alpha_i - \alpha_j|\,, \tag{34}$$

where μ_1 and μ_2 are the corresponding weights. This matching extent is used to introduce the matching minutiae queue of the local structure. Since the local structure with the highest score does not have to be the truly matching minutia, for each minutia in the template palmprint the method provide *m* candidates of the matching minutiae based on the average of the similar extent of the matched minutiae in the local structure matching. Now, before carrying out the global matching the global datum mark is confirmed for the coordinate's calibration.

Firstly, a new template minutiae set and a new compared minutiae set are constructed with all the candidates pairs of matching. Then a matrix L_{MxN} where the element $l_{i,j}$ is the matching minutiae number taking the minutiae i and j as the temp datum marks and building global feature eigenvectors around of then is obtained. The corresponding minutiae pair which has the biggest matching minutia number is selected as the global datum mark.

The global matching is performed using the old minutiae sets, but first the coordinates calibration of all the minutiae is performed in the compared palmprint using the global datum marks. Firstly, the translation factors $\Delta x, \Delta y$ and the rotation factor α are computed using the global datum marks and then the minutiae are calibrated obtaining a new compared set A'. The transformation formula is defined as:

$$\begin{bmatrix} x_i' \\ y_i' \\ \theta_i' \\ 1 \end{bmatrix} = \begin{bmatrix} \cos\alpha & -\sin\alpha & 0 & \Delta x \\ \sin\alpha & \cos\alpha & 0 & \Delta y \\ 0 & 0 & 1 & \alpha \\ 0 & 0 & 0 & 1 \end{bmatrix} \begin{bmatrix} x_i \\ y_i \\ \theta_i \\ 1 \end{bmatrix}. \tag{35}$$

The global matching is then performed using the new compared set A' and the template set B. A minutia $i \in A'$ match with a minutia $j \in B$ if the following conditions are met:

$$\left|x_i - x_j\right| < \delta_2 \,, \tag{36}$$

$$\left|y_i - y_j\right| < \gamma_2 \,, \tag{37}$$

$$\left|\theta_i - \theta_j\right| < \varepsilon_2 \,. \tag{38}$$

When one minutia matches with many others, the matching minutia pair with the smallest matching extent is chosen. The matching extent of two minutiae in the global matching phase is defined as:

$$M_g(i,j) = \left|x_i - x_j\right| + \left|y_i - y_j\right| + \mu_3\left|\theta_i - \theta_j\right| \,, \tag{39}$$

here μ_3 is weight value. The final score is computed by the following formula:

$$S = a * S_2 + b * \sum_{i=0}^{S_2} S_1^i + \sum_{i=0}^{S_2} \left(d - cS_3^i\right) \,, \tag{40}$$

where S_1^i is the matching number of neighborhood minutiae in the local structure of the matching pair i, S_2 is the number of matching minutiae pairs in the global matching phase, S_3^i is the difference of each matching pair with the coordinate transformation factor on the minutiae sets, a, b, c, d are weight values. Finally, the authors propose to use the reliability information of a minutia based on the quality of its position in the palmprint as a weight parameter to modify the final score.

This paper was improved by the same research group in [18]. In the step of constructing the local structure the formula to obtain the polar angle is modified; the new formula is as follows:

$$\varphi_i = \left(\frac{180}{\pi} \tan^{-1}\frac{y_i - y}{x_i - x} + 360\right) \%360 \,. \tag{41}$$

The selection of the global datum mark is done by selecting each candidate pair as a temporary datum mark, performing coordinate transformation and finally taking the pair that maximize the next formula:

$$C_{diff} = \frac{\sum_{i=1}^{N}\left(c_0 - (c_1\Delta x_i + c_2\Delta y_i + c_3\Delta\theta_i)\right)}{N} , \tag{42}$$

where N is the matching minutiae number and c_0, c_1, c_2, c_3 are weight parameters. After performing the coordinate transformation using the global datum mark the global matching is computed. The difference between two minutiae in the global matching phase is defined as:

$$G\_diff_i = g_0 + g_1 * M_i - g_2 * \begin{pmatrix} c_1 \\ c_2 \\ c_3 \end{pmatrix}\begin{pmatrix} \Delta x_i \\ \Delta y_i \\ \Delta\theta_i \end{pmatrix}, \tag{43}$$

here g_0, g_1 and g_2 are weight values. The final score is computed as:

$$S = \frac{\sum_{i=1}^{n} G\_diff_i}{G_{MAX} * n} * MAX , \tag{44}$$

where n is the minutia number in the template palmprint, G_{MAX} is the maximum value of G_diff and MAX is the maximum value of S. The above approaches are not very robust to distortion and spurious minutiae. Consequently the results reported in the experiments are very poor in partial-to-full palmprint matching.

In [19] a latent-to-full palmprint high resolution matching method more robust to distortion and spurious minutiae than the previous was presented, based in a similar approach for fingerprint [20] that use radial triangulation to modeling the minutiae local structure. A local structure based on radial triangulation is showed in Figure 15 that was taken from [19].

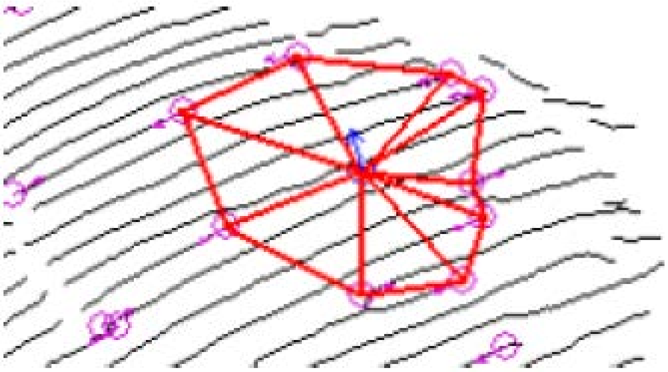

Fig. 15. A local structure of a minutia based on radial triangulation [19].

Given a minutia $p(x, y, \theta)$ called centroid, the eigenvector of its local structure with k minutiae based on radial triangulation is described as:

$$LS = \left[x, y, \theta, V_1, R_1, L_{1,2}, ST_{1,2}, V_2, R_2, L_{2,3}, ST_{2,3} \ldots V_k, R_k, L_{k,0},, ST_{k,0}\right] , \tag{45}$$

where V_k is the vertex of the minutia k, R_k is the radius of minutia k to the centroid, $L_{k,k+1}$ is the length of the polygon side between minutia k and minutia $k+1$ and $ST_{k,k+1}$ is the area of the triangle defined by the minutiae $k,\ k+1$ and the centroid. Each vertex V_k of the polygon is transformed into the polar coordinate system of the centroid in the same way as in [18], they only modified the relative direction formula as follows:

$$\alpha_k = \big((\theta_k - \theta) + 360\big)\%360\,. \tag{46}$$

In the local matching stage local minutiae sets of N minutiae are firstly selected to build the radial triangulation structures. The selection is done by sorting the minutiae in ascending order of the distances to the origin of the coordinate system. The minutia nearest to the origin and the $N-1$ minutiae nearest to it are selected. The process is repeated considering the minutiae not selected until the number of remaining minutiae is less than N. Then for each set of N minutiae a radial triangulation structure is constructed.

A pair of local structures is considered a matched pair when the following conditions are met:

$$\frac{1}{N^2}\sum_{i=1}^{N}\sum_{k=1}^{N}\sqrt{(\rho_i\cos\varphi_i - \rho_k\cos\varphi_k)^2 - (\rho_i\sin\varphi_i - \rho_k\sin\varphi_k)^2} \le DV_0\,, \tag{47}$$

$$\frac{1}{N^2}\sum_{i=1}^{N}\sum_{k=1}^{N}|R_i - R_k| \le DR_0\,, \tag{48}$$

$$\frac{1}{N^2}\sum_{i=1}^{N}\sum_{k=1}^{N}|L_i - L_k| \le DL_0\,, \tag{49}$$

$$\frac{1}{N^2}\sum_{i=1}^{N}\sum_{k=1}^{N}|ST_i - ST_k| \le DST_0\,, \tag{50}$$

where the minutia indexed by i are the minutiae of the local structure of the latent print and those indexed by k are the minutiae of the local structure of the full print, DV_0, DR_0, DL_0 and DST_0 are the average values for all the local structure pairs. The similarity between two minutiae (l,f) in the paired structure is defined as:

$$S_m(l,f) = \frac{\frac{1}{N^2}\sum_{i=1}^{N}\sum_{k=1}^{N}\sqrt{(\rho_i\cos\varphi_i - \rho_k\cos\varphi_k)^2 - (\rho_i\sin\varphi_i - \rho_k\sin\varphi_k)^2}}{\sqrt{\left(\rho_l\cos\varphi_l - \rho_f\cos\varphi_f\right)^2 - \left(\rho_l\sin\varphi_l - \rho_f\sin\varphi_f\right)^2}}\,. \tag{51}$$

The pairs of minutiae with the maximum value of similarity are marked as candidates. The ten minutiae pairs with the highest similarity are used to align the two sets of minutiae. Then in the global matching phase all the minutiae pairs are examined and those closest to each other in location and direction are deemed as the matched minutiae pairs. The final score is computed by the following formula similarly to [7]:

$$S = \frac{N_M}{N_M + 20} * S_D * \frac{N_M}{N_M + N_L} * \frac{N_M}{N_M + N_F}\,, \tag{52}$$

where N_M is the matched minutiae number, 20 is an experience value of the minimum number of matched minutiae for genuine comparison referred to [7], S_D is the average similarity of radial triangulation structures for all the matched minutiae, N_L and N_F denote the number of unmatched minutiae in latent and full palmprints.

This approach was improved by the same authors in [21]. They argued that their previous approach has the following unresolved problems:

1. The discriminative power of the similarity based on radial triangulation structure is not stable.
2. To select more accurate calibration centers, finer alignments based on global information is needed.
3. Learning based comparison score computation is needed to better distinguish between genuine and imposter.

In [21] their previous approach is improved by using the relaxation technique for point pattern comparison and use logistic regression learning for the final score computation. A new approach for the palmprints alignment is also introduced. The relaxation is used to modify the formula (51) as follows:

$$S_m(l,f) = \frac{1}{N-1}\sum_{p\neq l}\langle \max[\vartheta(|\delta_{l,f}(p,q)|) \mid q \neq l\,]\rangle\,, \tag{53}$$

where $\delta_{l,f}(p,q)$ denotes the position difference of p and q when l is mapped into f and $\vartheta(x) = 1/(1+x^2)$.

To perform the alignment, subsets of L minutiae are selected from the centroid set of the full palmprint, and from the latent palmprint centroid set only one subset of L minutiae. L is the number of radial triangulation structures in the latent palmprint. The selection is done using the same procedure that was used to select the sets of N minutiae for the local structures construction. Then for each set a simplified radial triangulation structure is constructed. For each simplified radial triangulation structure in the full palmprint the similarity between its centroids c_{f_n} and the centroids of the latent palmprint c_{l_m} is computed by applying the formula (53) to centroids. Then the support $p(c_{l_m}, c_{f_n})$ of the centroid pair gives to the structure pair is calculated by:

$$p(c_{l_m}, c_{f_n}) = \frac{S_m(c_{l_m}, c_{f_n})}{\sum_{n=1}^{L} S_m(c_{l_m}, c_{f_n})}\ . \tag{54}$$

To select the ten minutiae for the alignment procedure a modified similarity value using the support value described above is obtained. The modified similarity value is computed as:

$$S_0(l,f) = S_m(l,f) * p(c_{l_m}, c_{f_n})\,, \tag{55}$$

where the minutiae l and f are in the radial triangulation structures related to the centroids c_{l_m} and c_{f_n} respectively. The global matching phase is performed as described in [19]. Finally the score expression is modified by:

$$S = \gamma_0 + \gamma_1 * \frac{N_M}{N_M + 20} + \gamma_2 * S_D * \frac{N_M}{N_M + N_L} * \frac{N_M}{N_M + N_F}\,, \tag{56}$$

where γ_0, γ_1, γ_2 are parameters obtained by logistic regression learning [22]. The results reported shows how this proposal works better than the previous and the one proposed by Jain et al. (2009) which will be covered in the next chapter. Later we will present and discuss those results.

4 Multi Feature Partial Palmprint Matching Methods

In [23] two system for full-to-full palmprint matching and partial-to-full palmprint matching are proposed. The authors propose the use of a variety of palmar features (friction ridges, minutiae, flexion creases and palmar texture). In [23] a new segmentation algorithm based on Active Contour Model to distinguish the foreground from the background it is also introduced. In this section we will be covering the partial-to-full system while the full-to-full system will be cover in the next section.

In order to remove the spurious minutiae caused by creases, an algorithm based on different resolutions of the same palmprint image is developed to detect the creases map. Firstly, the ridge valley pattern is removed by applying a Gaussian smoothing filter width size window 15 and standard deviation 6. Also two palmprint images with resolution of 250 dpi and 125 dpi are obtained from the original image. Eight directional filters [24] are applied to convolve the three images obtaining a candidate crease region. Further processing is applied to the candidate crease region connecting the line segments close to each other by using the Radon transform [25]. After the minutiae extraction those minutiae close to a crease are removed.

The latent-to-full palmprint matching technique proposed in [23] uses the texture information in addition to the minutiae information. Texture information is captured using the Scale Invariant Feature Transformation (SIFT) [26] points. The argumentation to use SIFT points is that in some cases when minutiae matching fails completely SIFT provide a good similarity score.

The first step to extract the SIFT points is to obtain the Different of Gaussian (DOG) images by using a set of Gaussian smoothed original image at various scales, then they search for stable points in the DOG space. Then to obtain the feature points each pixel is compared with the neighborhood, and the ones with the smallest or the highest values are selected, those points lying on an edge are removed. Then a descriptor invariant to orientation is obtained by using the histogram of orientation gradient and rotating it with respect to the dominant orientation. Two points are deemed matched if the ratio of the Euclidean distance to the closest points is less than a threshold (0.75 in their experiments). The matching score is the number of matching points. VeriFinger 4.2 [9] is used to match the minutiae and both score are then combined.

The following limitations of the above procedure were pointed by [7] when they argued that the SIFT features cannot be consistently detected in latent and full prints and that VeriFinger 4.2 is not advisable for latent palmprint matching. We can also say that the computational cost of the algorithm is extremely high and that any algorithm to align the latent palmprint images is proposed. Furthermore, the number of SIFT points is extremely high and therefore the system is impractical in forensic scenarios.

In [7] the authors introduce a new fixed length minutia descriptor named MinutiaCode used to capture distinctive information around a minutia. This descriptor is based on a previous work [27] where the length of the minutia descriptor proposed is variable depending on the number of neighboring minutiae. The authors in [7] argue that the similarity between two variable-length minutiae descriptors is not very efficient, therefore a fixed-length minutia descriptor MinutiaCode is introduced.

The MinutiaCode of a minutia is constructed by dividing the circular region around a minutia into $(R-1)*K$ sectors by $R=5$ concentric circles and $K=8$ lines. The radius of the r circle is $20*r$ pixels. The direction of the k line is $\theta+(k-1)*\frac{\pi}{K}$, where θ denotes the direction of the central minutia. For each sector a set of features is computed, including the quality (1: foreground, 0: background), mean ridge direction, mean ridge period, and the numbers of four types of neighboring minutiae defined as: reliable and with the same direction as the central minutia (RS), unreliable and with the same direction as the central minutia (US), reliable and with the opposite direction to the central minutia (RO) and unreliable and with the opposite direction to the central minutia (UO). If the difference between the directions of the neighboring minutia and the central minutia is less than $\pi/2$, the neighboring minutia has the same direction to the central minutia, otherwise it has the opposite direction. To classify the minutiae in reliable and unreliable the procedure described in [28] is used.

The similarity s between two MinutiaCodes is defined as the weighted average value of the similarities of all valid sectors. A pair of sectors is considered valid if both sectors are in the foreground. If the numbers of valid sectors is less than $(R-1)*k/2$ then $s=0$ otherwise s is computed by:

$$s = \frac{1}{\sum_{i=1}^{(R-1)*k/2} w_i} \sum_{i=1}^{(R-1)*k/2} w_i s_i \, , \tag{57}$$

where s_i denotes the similarity of the i pair of sector and w_i the weight of the pair of corresponding sectors and is defined as $w_i = (\max(n_1, n_2) + w_0)$, where n_1 and n_2 are the number of reliable minutiae in the two corresponding sectors and w_0 is a weight for sectors without reliable minutiae (set to 0.2 in their experiments).

The similarity s_i between two corresponding sectors is defined as 0 if the difference between ridge directions or ridge periods is greater than the corresponding threshold ($\frac{\pi}{6}$ and 3 pixels), otherwise s_i is computed as:

$$s_i = \frac{n_M}{n_S} \, , \tag{58}$$

$$n_M = n_{MS} + n_{MO} \, , \tag{59}$$

$$n_S = n_{SS} + n_{SO} \, , \tag{60}$$

$$n_{MS} = \min(n_{RS1} + n_{US1}, n_{RS2} + n_{US2}) \, , \tag{61}$$

$$n_{MO} = \min(n_{R01} + n_{U01}, n_{R02} + n_{U02}) \, , \tag{62}$$

$$n_{SS} = \max(n_{RS1}, n_{RS2}, n_{MS}) \, , \tag{63}$$

$$n_{SO} = \max(n_{RO1}, n_{RO2}, n_{MO}) \, , \tag{64}$$

where n_M is the number of matched minutiae, n_S number of minutiae that should be matched and n_{RS}, n_{US}, n_{R0}, n_{U0} the number of minutiae in the palmprint of types RS, US, RO, UO respectively.

The global matching is performed using the normalized similarity defined in [28] and taking the top-five pairs of minutiae in decreasing order. These top-five pairs of minutiae are used to perform the alignment process. After the alignment, the minutiae close to each other in location and direction are classified as matching minutiae.

The matching score is computed as:

$$S = W_m * S_m + (1 - W_m) * S_d \, , \tag{65}$$

where S_m and S_d denote the minutiae matching and the direction field matching scores respectively. The weight W_m is empirically set to 0.8. The minutiae matching score is calculated by the formula (52), but now S_D is the average similarity of descriptors for all the matching minutiae, and N_L and N_F are the number of unmatched minutiae in latent and full prints that are reliable and belong to the common region of the two palmprints. The direction field matching score is computed by:

(66)

$$S_d = \frac{N_b}{N_b + 900} * \left(1 - \frac{2 * D_d}{\pi}\right),$$

where N_b is the number of blocks where the difference of direction between latent and full print is less than $\frac{\pi}{8}$, and D_d is the mean of the difference of direction values of all the blocks.

Some disadvantages of this proposal are pointed by the authors of [21]. They say that MinutiaCode is not robust to distortion and disturbance of central minutiae and also that is too time consuming.

In [14] a new method for latent palmprint matching is proposed, that makes use of a variety of features. These features are minutiae, orientation field, density map and principal lines.

In the minutiae extraction stage a value of confidence level is attached to the minutiae, based on the difference of the ridge direction produced by the composite algorithm that estimate the orientation field previously described in section 1 and the gradient-based method in the region around the minutia. If the difference is high the confidence level is low, otherwise the confidence level is high. Before the matching score is computed, the alignment procedure is performed using the method proposed in [29]. The matching minutiae score is computed by:

$$S_m = \frac{C_m}{C_m + 20} * \frac{C_m^2}{C_l C_f}, \tag{67}$$

where C_m is the sum of all the matched minutiae pairs confidence level productions, and C_l and C_f are the sum of all the confidence value in the common area for latent and full palmprint respectively.

The density map is extracted along with the orientation field and the similarity score is calculated as:

$$S_d = \frac{N_d}{N_d + 900} * \frac{1}{N_b} \sum_{(x,y)\epsilon\nabla} exp\left(-\left|\frac{1}{f_l(x,y)} - \frac{1}{f_f(x,y)}\right|\right), \tag{68}$$

where N_d is the number of matched blocks, ∇ denotes the common area, N_b is the number of blocks in the common area, and f_l and f_f denote the ridge densities of latent and full palmprints respectively. A matched block pair is composed by two overlapping blocks whose ridge distance (the inverse of ridge density) difference is within 1 pixel. The similarity of the orientation fields S_o is measured with a similar score formula.

To extract the principal lines map they need to distinguish the principal lines from all the detected creases in their estimation of the orientation field. To achieve this, the general Hough transform [30] is applied. The similarity of the principal line map is computed by the next formula:

$$S_p = \frac{E_m}{\min(E_l, E_f)}, \tag{69}$$

$$E_m = \sum_{(w,h)} \min\{I_E^l(w,h), I_E^f(w,h)\} * \left|I_D^l - I_D^f\right|, \tag{70}$$

where E_l and E_f are the principal line energy sum in the common area for latent and full palmprint respectively, I_E^l and I_E^f are the creases energy of the matched energy points and I_D^l and I_D^f are the directions of these matched points. Two energy points are deemed as matched if they are located at the same position and the direction difference between their corresponding principal lines is less than $\frac{\pi}{6}$.

For the scores fusion two different techniques are proposed for verification and identification tasks. In verification the linear weighted sum of all the scores is computed and then SVM is used as a classifier to distinguish between a genuine score and an impostor score. For identification purposes the authors cited a previous work [31] that stated that the weighted sum performance deteriorates if the features are conditionally correlated. Therefore the correlations of the different features are analyzed to introduce a new heuristic rule. As minutiae and density map are of low correlation both features are fused as following:

$$S_{md} = w_m S_m + (1 - w_m) S_d \,. \tag{71}$$

To fuse the principal line map, the authors argued that although its discriminative power is worse than the other features, it can provide independent global information of the palmprint. The similarity score of the above tree features is computed as:

$$S_{mdp} = S_{md} + S_{md} * \frac{1}{1 - S_p} \,. \tag{72}$$

Since the orientation field is heavily correlated with the minutiae then the final fusion score is defined as:

$$S = S_{mdp} + S_{mdp} * S_{o\,.} \tag{73}$$

One of the main drawbacks of this proposal is that the information related to principal line is not always presented in a latent palmprint so this information seems to be unnecessary in latent-to-full palmprint matching but not in full to full palmprint matching. Furthermore even when the results in partial-to-full tests outperform the results obtained in [7] the computational complexity remains extremely high. One important result of this work is that it proved that other kinds of features can be used effectively with minutiae information even though the system was not tested with latent palmprints.

In [32] a match propagation minutiae algorithm was introduced. The idea is that for a genuine pair of matched minutiae belonging to a pair of genuine matched palmprints the surrounded minutiae should also match with high confidence, and for an impostor pair of palmprints the matched minutiae may appear at arbitrary locations in the palmprint image. Before the match propagation algorithm, a clustering algorithm is applied on the minutiae to avoid similarity computation between minutiae with different local characteristics.

To describe the local properties of the minutiae orientation structure proposed in [33] is used. Given a reference minutia m, L concentrical circles are considered to extract the local information about the minutia m. L sample points are equally distributed for each circle starting from the projection location of m along its direction on the circle. The value of each sample point is the difference of the local ridge orientation at the sample point and the ridge orientation at the location of reference minutia. The ridge period descriptor is also taken into account at that point. This local descriptor is invariant to translation and rotation. Some sample may fall outside the foreground region, so the values of this sample points are estimated with the next formulas:

$$o = \frac{1}{2} \tan^{-1} \left(\frac{\sum_{i \in V} \sin 2o_i}{\sum_{i \in V} \cos 2o_i} \right), \tag{74}$$

$$w = \frac{1}{n_v} \sum_{i \in V} w_i \,, \tag{75}$$

where V is the set of valid nearest sample points with n_v points in the structure, o and w are the predicted ridge orientation and ridge period values. The distance between two orientation descriptors is computed by:

$$D(OD, OD') = \sqrt{\sum_{i=1}^{N} [(\cos 2o_i - \cos 2o'_i)^2 + (\sin 2o_i - \sin 2o'_i)^2]} \ , \tag{76}$$

where N is the number of sample points. The centroid of the cluster with S descriptors is defined as:

$$c_i = \frac{1}{2}\tan^{-1}\left(\frac{\sum_{k=1}^{S} \sin 2o_k}{\sum_{k=1}^{S} \cos 2o_k}\right) . \tag{77}$$

The clustering for ridge orientation descriptors is done by using K-means as in the case of ridge period descriptors. In the last case the Euclidean distance measure is used. The minutiae are also clustered by assigning each minutia to the cluster whose centroid is closest to the minutia descriptor.

For the minutiae based comparison they defined three minutiae similarity measures. The first two are based on ridge orientation and ridge period descriptors and are defined as:

$$S_o = \frac{1}{N_v}\sum_{i \in V} exp\left(-\frac{\Delta o_i}{\mu_o}\right) , \tag{78}$$

$$S_r = \frac{1}{N_v}\sum_{i \in V} exp\left(-\frac{\Delta w_i}{\mu_r}\right) , \tag{79}$$

$$\Delta o_i = min(|o_i - o'_i|, 180 - |o_i - o'_i|) , \tag{80}$$

$$\Delta w_i = |w_i - w'_i| , \tag{81}$$

where V is the set of sample points valid in both descriptors (the predicted sample points values are not used), N_v is the number of valid sample points, and μ_o and μ_r are two predefined parameters set to 4 and 2 respectively. When $N_v < 20$ $S_o = S_r = 0$. The third measure computes the similarity between the local structures of two minutiae. The local structures are constructed in a similar way than [7] that was previously described in this work, with the slight difference that the sectors in the template palmprint are overlapped. Each minutia in the local structure of a center minutia is described by the triplet (r, γ, α) where r and γ are the radius and the angle in the polar coordinate system respectively, α is the normalized minutia direction. These values are taken with respect to the center minutia and the center minutia direction respectively. After the alignment of the two structures two minutiae in the same sector are deemed as matched minutiae if the following three conditions are met:

$$min(|\gamma - \gamma'|, 360 - |\gamma - \gamma'|) < TH_\gamma , \tag{82}$$

$$|r - r'| < \frac{r}{r_{max}} * TH_r , \tag{83}$$

$$min(|\alpha - \alpha'|, 360 - |\alpha - \alpha'|) < TH_{\alpha}, \tag{84}$$

where TH_{γ}, TH_r and TH_{α} are thresholds set by them to 15, 20 and 8 respectively, r_{max} is the radius of the local structure. The Euclidean distance is used to select one pair of minutiae from those pair of minutiae that satisfy the above conditions. The similarity of two local structures is given by:

$$S_m = \frac{1}{M}\sum_{i=1}^{M} s_i * \frac{M}{N_t + N_q} * \frac{M}{M+10} * Q(d_q) * Q(d_t), \tag{85}$$

where M is the number of matched minutiae, N_q and N_t are the numbers of local minutiae in the query and the template respectively, s_i is the similarity of the i minutiae pair, $Q(x)$ is the minutiae quality measure defined in [34] and d_q and d_t are the average Euclidean distances of the three nearest minutiae to the center minutiae in query and template structures respectively.

After the minutiae clustering, the next step is to select the initial minutiae pairs for the match propagation process. The algorithm is as follows:

1. For each cluster, the weak similarity between each minutia in the query palmprint and each minutia in the template palmprint is computed, the pair with the highest weak similarity is selected. Weak similarity is computed as: $S_o * S_r$.
2. The top K minutiae pairs with the highest weak similarity are selected. K is defined as: $\min(100, M_q)$ where M_q is the number of minutiae in the query palmprint.
3. For each minutiae pair selected in the above step, their strong similarity are computed. Strong similarity is defined as: $S_o * S_r * S_m$.
4. Select the top K' minutiae pairs with the highest strong similarity. K' is defined as: $\min(50, K)$.
5. The top K' minutiae pairs selected are the initial minutiae pairs for the match propagation process.

The matching propagation procedure for an initial minutiae pair is as follows:

1. For the initial pair the matching minutiae in their local structure are selected.
2. Each matching minutiae pair with no minutiae already selected is added to the minutiae matching list result.
3. The pairs of minutiae selected above whose strong similarity is bigger than a threshold and their transformation parameters are close enough to the transformation parameters of the initial pair are selected for the match propagation process and are stacked for further process.
4. One pair of those stacked is selected as the new initial pair and then the algorithm is repeated from the step 1 until there are not more pairs stacked.

Next the score of the overlapped region determined by the minutiae pairs given by the above procedure is calculated. To compute the score they used the orientation field ($Score_o$), the density map ($Score_r$) and the average minutiae similarity ($Score_m$):

$$Score_o = \frac{1}{N_b}\sum_{i=1}^{N_b} exp\left(-\frac{\Delta o_i}{\mu_o}\right) * \frac{N_o}{N_o + 900}, \tag{86}$$

$$Score_r = \frac{1}{N_b}\sum_{i=1}^{N_b} exp\left(-\frac{\Delta r_i}{\mu_r}\right) * \frac{N_r}{N_r + 900}, \tag{87}$$

(88)

$$Score_m = \sum_{i=1}^{M} Sim_{orm}^{i} ,$$

$$Score = Score_o * Score_r * Score_m , \tag{89}$$

where N_b is the number of blocks of 16X16 pixels in the overlapped area, N_o is the number of blocks with the average ridge orientation difference less than 22.5 degree, N_r is the number of blocks with the average ridge period difference less than 2 pixels and Sim_{orm}^{i} is the strong similarity of the i pair computed by the match propagation process.

If the score obtained is bigger than a predefined threshold then this is deemed as the final score and no more processing is needed, otherwise the match propagation algorithm is performed again using another initial pair of minutiae. If none of the obtained scores is bigger than the predefined threshold then the final score is the maximum of the obtained scores.

The above approach has no need of any ridged alignment which constitutes one of its bigger advantages. The results obtained not only improve the previous results in [7] but also the clustering procedure makes the current approach more efficient. However the system still remains very susceptible to spurious minutiae and small overlap area.

In [35] the authors argued that even when the use of radial triangulation [19, 21] increases the accuracy, the features extracted from them, are still affected by skin distortion. They proposed the use of a representation called expanded triangle set [36], which is based on minutia triplets obtained from Delaunay triangulation. The use of the expanded triangle set is justified by the high affectations in the Delaunay triangular structure caused when the extraction method fails to find a minutia.

Given a set of points P, a Delaunay triangulation T over that set of points and E the set of edges of the Delaunay triangulation the expanded triangle set is defined as:

- Definition 1 (Triangular Hull). Let p_i be a point of P. The set $N_i = \{p_j | (p_i, p_j) \epsilon E\}$ denoted the points set formed by all the adjacent vertices of p_i in the Delaunay graph G. the triangular hull of p_i is defined as the Delaunay triangulation of the planar point set N_i, and it is denoted by H_i.
- Definition 2 (Expanded triangle set). The expanded triangle set of P is defined as $R = T \cup H_1 \cup H_2 \cup \ldots \cup H_N$.

Therefore the set R contains all of the Delaunay triangles that are formed when each minutia is eliminated individually. Figure 16 shows some triangle sets examples.

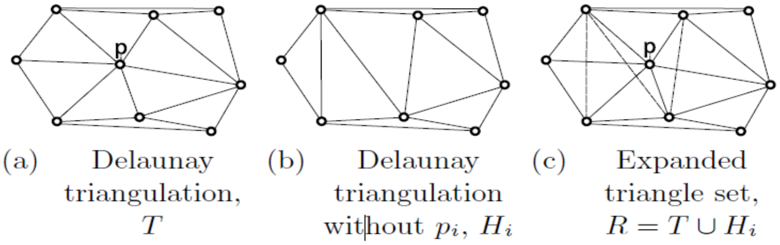

(a) Delaunay triangulation, T (b) Delaunay triangulation without p_i, H_i (c) Expanded triangle set, $R = T \cup H_i$

Fig. 16. Triangle sets examples [35]

For each triangle t in the expanded set, they defined a feature vector $f(t)$ as follows:

$$f(t) = (s_t, \beta_1, \beta_2, \beta_3, r_1, r_2, r_3, d_1, d_2, d_3) , \tag{90}$$

$$s_t = \begin{cases} 0, & A_t < 0 \\ x, & otherwise \end{cases} , \tag{91}$$

$$A_t = x_1(y_2 - y_3) + x_2(y_3 - y_1) + x_3(y_1 - y_2)\,, \tag{92}$$

where s_t is the triangle sign which is invariant to rotation, β_i is the relative direction of the minutia m_i with respect to his opposite side in t, r_i is the ridge counter between minutiae (number of ridges crossed by a triangle side joining two minutiae) and d_i is the length of the i side of the triangle. After the feature extraction they remove from the expanded set the triangles with at least one of value of r_i outside the interval [0,16).

Two feature vectors $f(t)$ and $f(t)'$ are corresponding if the following conditions are met:

$$s_t = s'_{t}\,, \tag{93}$$

$$|\beta_i - \beta'_i| \leq \delta_{\beta}\,, \tag{94}$$

$$|r_i - r'_i| \leq \delta_r\,, \tag{95}$$

$$|d_i - d'_i| \leq \delta_d\,, \tag{96}$$

where δ_β, δ_r, δ_d are predefined thresholds set to 3 in their experiments. The tuples of two corresponding triangles t and t' are defined as $ct_i = (\alpha_i, e_i, e'_i)$ where α_i is the normalized difference between the i interior angles of t and t' computed in a similar way to [37] and e_i, e'_i are segments of the triangles. They take only those tuples with α_i equal to the mode of all corresponding tuples. Those tuples are used to build a similarity weighted graph G_s.

The vertices set of G_s is built from the minutiae that originate the segments of the tuples and the edges set is built from the mutual match between the same segments. That is to say, for each tuple the two vertices that originate the segments are added to the vertices set if they are not previously added, an edge connecting these two vertices is added too. A similarity value between two segments of a tuple is added as a weight value to its corresponding edge. The graph G_s could not be connected; therefore they applied the Kruskal algorithm to find the spanning tree of every connected component. The spanning trees are sorted by the number of edges. The first spanning tree is merged with the second by trying to add a virtual edge that met some additional geometrical constraints if this process is successful the merged spanning tree is taken as the first spanning tree and the process is repeated until no more spanning trees can be merged. The final score between a query palmprint M_q and a template palmprint M_t is given by:

$$S(M_q, M_t) = \frac{sim * |V|}{\min(|M_q|, |M_t|)}\,, \tag{97}$$

where $|V|$ is the number of vertices in the similarity graph G_s, $|M_q|$ and $|M_t|$ are the number of minutiae in the query palmprint and in the template palmprint respectively, and sim is the sum of the weights of all the edges in the merged spanning tree.

5 Full-to-Full High Resolution Palmprint Matching

Full-to-Full high resolution palmprint matching methods are mainly used in authentication platforms when a high reliability is needed because of the high cost of the acquisition devices. In [23] before the minutiae matching (See previous section), the two compared palmprints are coarsely aligned by the heart line. The resolution of the segmented image is reduced to 125 dpi and the upper left region of the down-sampled image is cut. To detect the heart line from the cropped image the 2D Morlet wavelet transform [38] and the Random Sample Consensus algorithm (RANSAC) [39] are applied. The 2D Morlet wavelet transform is used to capture the high frequency responses where the intensity values change abruptly, while the RANSAC algorithm is used to fit a line to the response set of point.

After the alignment the palmprint image is divided in 5 sectors as they show in the Figure 17, the point P is the starting point of the heart line estimated in the above step. The minutiae matching process is performed by VeriFinger 4.2 [9].

In [8] the authors did three major contributions to the field of palmprint matching:

1. A quantitative study about the discriminative power of various palmprint features in the different regions. Some results of this study were cited in the introduction of this work.
2. For the alignment of the enrolment palmprints process an orientation field based algorithm is introduced.
3. A segmented-based palmprint matching algorithm to deal with the different discriminative power of the different palmprint regions and distortion.
4. A cascade filtering to reject non matched palmprints in an early stage.

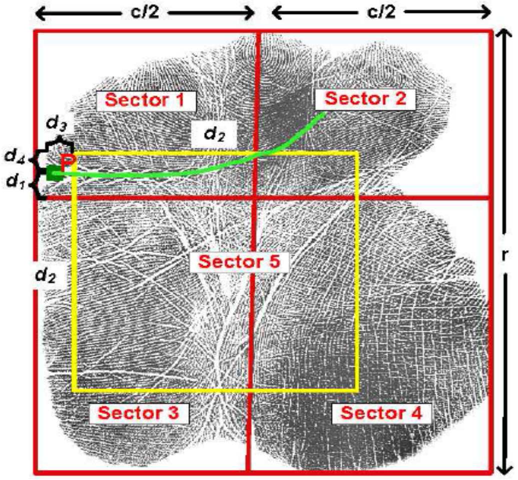

Fig. 17. Sector division in [23].

In their study they founded, as was defined by palmprint forensic experts in [40], that there is some common patterns in palmprints with low deviation for each palmar region and a high deviation between regions. The Figure 13 taken from [8] shows the common patterns of the ridge flow in the different regions. Therefore they argue that orientation field is a good feature for the alignment of the palmprints in the enrollment stage. The Figure 18 is used as a reference for the alignment in the enrollment stage. The reference image is also mirrored and used to classify the enrollment palmprints in left palmprints or right palmprints. To obtain the transformation parameters the generalized Hough transform [30] is applied and high weights are assigned to the regions with high orientation field consistence.

In the segmented-based matching algorithm each registered palmprint is firstly divided into 16 non-overlapped segments of 510x510 pixels. This segmentation is also performed in the query palmprint and each segment is matched with the corresponding segments in the template database. Before the match, each template segment is enlarged to 610x610 pixels with the aim of completely contain the query segment, and then, those pair of segments with a small foreground and minutiae in the overlapped section (incomplete segments) are removed. Finally, the remaining pair of segments are aligned using the Hough transform minutiae matching algorithm described in [29].

After the align process, the similarity of each feature (minutiae, orientation field, density map) is obtained in the aligned pair of segments respectively. The values of similarity of minutiae and density map are computed similarly to [14] using the formulas (67) y (68) respectively. The similarity of the orientation field is estimated with the following formula:

$$S_o = \frac{N_o}{N_o + 100} * \left(1 - \frac{D_o}{90}\right), \tag{98}$$

where N_o is the number of matched blocks by its orientation field and D_o is the mean of the orientation difference in all the blocks. At this point, the relative displacement of each pair of segments are also used as a feature. Therefore the feature vector has 96 components taking into account each similarity value and relative difference for each pair of segments.

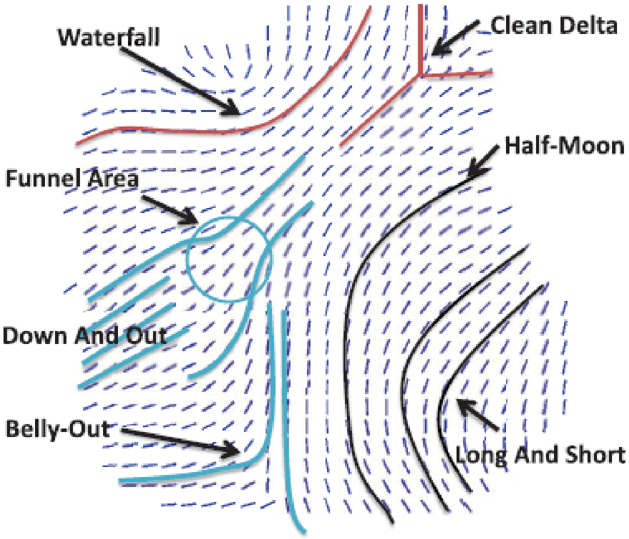

Fig. 18. The common patterns of the ridge orientation flow in different regions of a palmprint [8].

Finally a Bayesian Framework is used to estimate a match score. The likelihood ratio is estimated with the next formula:

$$L = \frac{P(G)}{P(I)} \prod_{k=1}^{16} \left(\epsilon + L_k^s L_k^d\right), \tag{99}$$

where $P(G)$ and $P(I)$ are the priori probabilities of be a genuine or an impostor respectively, L_k^s and L_k^d are the likelihood ratio values estimated according to the similarity scores and displacements parameters of the k pair of segments respectively and ϵ is a regularization term empirically set to 0.001 added to avoid the influence of very poor quality segments on genuine matches. The values $\frac{P(G)}{P(I)}$ and the likelihood of the incomplete segments are set to 1. They use Gaussian Mixture Models (GMMs) and Expected Maximization (EM) to train the Bayesian framework.

A cascade filter is also proposed to reject those palmprints with some unmatched segments. The idea is to reject the most pair of palmprints by just comparing a small region. Then in each level of the cascade filter the likelihood of the query palmprint segments with the segments of cascade filter level is estimated and if this value is bigger than some threshold defined for this level then the palmprint is passed to the next level otherwise is rejected.

The global procedure described above is applicable to full-to-full palmprint matching. In latent-to-full palmprint matching it requires a manually alignment by a forensic expert. The above statement and the fact that this algorithm is essentially designed for full-to-full palmprint matching [32] is the reason why it was presented in this section.

In [41] a palmprint matching algorithm based on the Minutia Cylinder-Code representation proposed in [42] is introduced. MCC is a fixed-radius approach based on 3D data structures that can be represented by a bit vector and therefore is very efficient for matching purposes. The only different with the MCC descriptor proposed in [42] is that for achieve better efficient, the validity record of each MCC descriptor component is removed. The similarity between two local structures is computed as was described in [42].

The global score is computed by means of a relaxation matching strategy. Given all the local similarities they firstly obtain a normalized similarity matrix as:

$$\hat{S}[r,c] = \left(1 - \frac{\sum_{i=1,i\neq r}^{n_A} S[i,c] + \sum_{j=1,j\neq c}^{N_B} S[r,j]}{n_A + n_B - 2}\right) * S[r,c]\,, \tag{100}$$

where n_A and n_B are the number of minutiae in palmprints A and B respectively, and $S[r,c]$ is the local similarity between the minutiae r and c. The idea is to update each similarity value taking into account the similarity of each minutia with all the minutiae in the other palmprint with the aim of penalize the minutiae that are not too much discriminant (i.e. minutiae having high similarity values with many others). Then the top n_R minutiae pairs are selected for the relaxation process.

The normalized similarity of a pair of minutia t at iteration i in the relaxation procedure is defined as:

$$\hat{S}_t^i = w_R * \hat{S}_t^{i-1} + (1 - w_R) * \frac{\left(\sum_{k=1,k\neq t}^{n_R} p(t,k) * \hat{S}_k^{i-1}\right)}{n_R - 1}\,, \tag{101}$$

$$p(t,k) = \prod_{i=1}^{3} Z\left(d_i, \mu_i^{\rho}, \tau_i^{\rho}\right), \tag{102}$$

$$d_1 = \frac{\left|d_s\left(a_{r_t}, a_{r_k}\right) - d_s\left(b_{c_t}, b_{c_k}\right)\right|}{\max\left(d_s\left(a_{r_t}, a_{r_k}\right), d_s\left(b_{c_t}, b_{c_k}\right)\right)}\,, \tag{103}$$

$$d_2 = \left|d_{\emptyset}\left(d_{\theta}\left(a_{r_t}, a_{r_k}\right), d_{\theta}\left(b_{c_t}, b_{c_k}\right)\right)\right|\,, \tag{104}$$

$$d_3 = \left|d_{\emptyset}\left(d_R\left(a_{r_t}, a_{r_k}\right), d_R\left(b_{c_t}, b_{c_k}\right)\right)\right|\,, \tag{105}$$

where w_R is a weighting value in the interval [0,1], $d_{\emptyset}$ is the difference (modulo 2π) between two angles, d_{θ} is the directional difference between two minutiae, Z is a sigmoid function with parameters μ and τ and d_R is the radial angles difference. The radial angle is defined as the angle subtended by the edge connecting the two minutiae and the direction of the first one. Finally the global score is computed as the average of the n_p relaxed similarity values of the n_p pairs with the greatest efficiency E_t. The efficiency of pair t is defined as the ratio between the final and the initial value of similarity of t. As is easily see this procedure make specially emphasis in the angles and direction of the minutiae which can be problematic in palmprints with low quality. The results reported are obtained under full-to-full palmprint matching conditions and that is the reason why this approach was included in this chapter.

6 Conclusions

Summing up, high resolution palmprint matching is still a wide open field of research with a huge impact in the forensic field. The existing differences between palmprints and fingerprints make palmprint matching a more challenging problem and encourage the development of new techniques that can exploit the palmprints intrinsic characteristics. The literature available is yet very sparse compared with others fields despite the significant advances that have been made.

Orientation estimation algorithms are an important part in any fingerprint matching system. In palmprints, those algorithms have a bigger importance since the presence of a wide number of creases can lead to a non-reliable orientation estimation and therefore to the detection of many spurious minutiae. The orientation estimation algorithm proposed in [7] can be considered as the state-of-the-art algorithm in the field but yet it has some drawbacks associated to the region growing procedure:

1. The algorithm cannot reliably detect ridges in noisy high curvature areas.
2. If the region with the most reliable first waves was obtained from a crease seed, then the procedure fails in detecting the ridge region.
3. If a region obtained from a crease seed has no overlapping blocks with the ridge regions, then this region is copied to the final region and therefore the final region contains creases.

In general the algorithm described in [7] has some problems in areas with a very high density of creases. In [14] the authors proposed the use of the Radon transform to reliable extract ridges in those areas but the detection improvement reported is very small and the algorithm is considerably less efficient. Furthermore the problems associated to the region growing algorithm still remain. The use of more effective orientation estimation algorithms could lead to better recognition rates in the thenar region.

Triangulation methods [19, 21, 35] seem like a right approach to palmprint matching. They could make use only of minutiae position and direction information, features that can be reliable extracted by forensic experts. The experiments carried on [35] shows how their proposal outperforms the other triangulation methods proposed in the literature and the algorithm described in [7] (See Table 1). Nevertheless, there are some details to take into consideration:

1. The database used in the experiments contains only 22 latent impressions what raises the concern about the statistic stability of the results.
2. The proposal in [35] still has some problems associated to the spurious minutiae and the size of the connected components.
3. In [35] the authors make use of the number of ridges crossed by an edge, but we believe that this feature can be removed without any significant loss of effectiveness since the ridge counter is not a very robust feature for latent impressions.

   The results obtained in [35] were achieved without using any preprocessing or post processing technique.

Table 1. Comparison results of identification rate reported in [35]

Algorithms	Rank-1	Rank-10	Rank-20
Jain et. al. (2009) [7]	67%	73%	80%
Wang et al. [19]	63%	68%	72%
Wang et al. [21]	69%	78%	82%
Expanded Triangle Set [35]	77%	82%	82%

Many other features besides minutiae appear in the literature (i.e. SIFT points, orientation field, ridge density map and others) as well as some studies about their discriminatory value. For example, Dai and Zhou in [14] reported that unlike fingerprint the discriminatory power of ridge density map is bigger than the orientation field in palmprints. The discriminative power of the different palm regions had been also studied by several authors, the results indicate that the thenar region has the lowest discriminative power mainly due to the high density of creases and wrinkles. Jain et al. in [7] theorizes that creases can be used to improve the matching accuracy of the latent palmprint matching methods.

In [32] Liu et al. proposed an efficient latent-to-full palmprint matching method robust to the non-linear distortion that outperforms several other approaches both in accuracy and efficiency. However, the algorithm is still sensible to spurious minutiae and small overlap between impressions. The MCC based method for palmprint matching [42] performed very well in the FVC-onGoing 2012 competition beating in accuracy the algorithm proposed in [32] under partial-to-full conditions but we believe that a test under latent-to-full conditions is mandatory to give the final conclusion.

In conclusion, many of the algorithms proposed to partial-to-full palmprint matching are not tested in latent-to-full conditions. This is mainly because there are no public databases of latent palmprints. Spurious minutiae and small overlap area are today the most difficult problems in latent-to-full palmprint matching. One interesting problem that could lead to better accuracy and efficiency in latent palmprint matching is the automatic determination of to which palm region a particular latent impression belongs.

Future lines of work in this biometric area may be oriented to:

- Improve the effectiveness of the orientation field estimation methods with the aim of reduce the detection of spurious minutiae caused by the presence of creases.
- Develop a new algorithm for latent-to-full palmprint matching using only minutiae information. Explore the use of multiple features like creases to improve the effectiveness of the previously developed algorithm.
- Identify the region of the palm at which a given latent print belongs.

References

1. Coetzee, L., Botha, E.C.: Fingerprint recognition in low quality images. Pattern Recognition 26, 1441-1460 (1993)
2. Kong, A., Zhang, D., Kamel, M.: Palmprint identification using feature-level fusion. Pattern Recognition 39, 478-487 (2006)
3. Ashbaugh, D.R., Press, C.: Quantitative-qualitative friction ridge analysis: an introduction to basic and advanced ridgeology. CRC press Boca Raton (1999)
4. Zhang, D., Shu, W.: Two novel characteristics in palmprint verification: datum point invariance and line feature matching. Pattern Recognition 32, 691-702 (1999)
5. Maio, D., Jain, A.K.: Handbook of Fingerprint Recognition. Springer (2009)
6. Dewan, S.K.: Elementary, Watson: Scan a Palm, Find a Clue. The New York Times (2003)
7. Jain, A.K., Feng, J.: Latent palmprint matching. Pattern Analysis and Machine Intelligence, IEEE Transactions on 31, 1032-1047 (2009)
8. Dai, J., Feng, J., Zhou, J.: Robust and efficient ridge-based palmprint matching. Pattern Analysis and Machine Intelligence, IEEE Transactions on 34, 1618-1632 (2012)
9. Neurotechnology Inc: VeriFinger, http://www.neurotechnology.com.
10. Wang, R., Ramos, D., Fierrez, J., Krish, R.P.: Towards Regional Fusion for High-Resolution Palmprint Recognition. In: Graphics, Patterns and Images (SIBGRAPI), 2013 26th SIBGRAPI-Conference on, pp. 357-361. IEEE
11. Neurotechnology Inc: MegaMatcher 4.0 SDK, http://www.neurotechnology.com. (2011)
12. Stock, R., Swonger, C.: Development and evaluation of a reader of fingerprint minutiae. Cornell Aeronautical Laboratory, Technical Report CAL no. XM-2478-X-1 13-17 (1969)
13. Funada, J.-i., Ohta, N., Mizoguchi, M., Temma, T., Nakanishi, K., Murai, A., Sugiuchi, T., Wakabayashi, T., Yamada, Y.: Feature extraction method for palmprint considering elimination of

creases. In: Pattern Recognition, 1998. Proceedings. Fourteenth International Conference on, pp. 1849-1854. IEEE

14. Dai, J., Zhou, J.: Multifeature-based high-resolution palmprint recognition. Pattern Analysis and Machine Intelligence, IEEE Transactions on 33, 945-957 (2011)
15. Huang, D.-S., Jia, W., Zhang, D.: Palmprint verification based on principal lines. Pattern Recognition 41, 1316-1328 (2008)
16. Wan, D., Zhou, J.: Fingerprint recognition using model-based density map. Image Processing, IEEE Transactions on 15, 1690-1696 (2006)
17. Li, J., Shi, G., Feng, Q., Wan, H.: A New Point Pattern Matching Method for Palmprint. In: Artificial Intelligence and Pattern Recognition, pp. 302-306.
18. Tan, Z., Yang, J., Shang, Z., Shi, G., Chang, S.: Minutiae-Based Offline Palmprint Identification System. In: Intelligent Systems, 2009. GCIS'09. WRI Global Congress on, pp. 466-471. IEEE
19. Wang, R., Ramos, D., Fierrez, J.: Latent-to-full palmprint comparison based on radial triangulation under forensic conditions. In: Biometrics (IJCB), 2011 International Joint Conference on, pp. 1-6. IEEE
20. Neumann, C., Champod, C., Puch-Solis, R., Egli, N., Anthonioz, A., Bromage-Griffiths, A.: Computation of likelihood ratios in fingerprint identification for configurations of any number of minutiae. Journal of Forensic Sciences 52, 54-64 (2007)
21. Wang, R., Ramos, D., Fierrez, J.: Improving radial triangulation-based forensic palmprint recognition according to point pattern comparison by relaxation. In: Biometrics (ICB), 2012 5th IAPR International Conference on, pp. 427-432. IEEE
22. Kleinbaum, D.G., Klein, M.: Logistic regression: a self-learning text. Springer (2010)
23. Jain, A., Demirkus, M.: On latent palmprint matching. Tech. Rep. 48824, Michigan State University (2008)
24. Leung, T., Malik, J.: Representing and recognizing the visual appearance of materials using three-dimensional textons. International Journal of Computer Vision 43, 29-44 (2001)
25. Bracewell, R.N.: Two-dimensional imaging. Prentice Hall, New Yersey (1995)
26. Lowe, D.G.: Distinctive image features from scale-invariant keypoints. International Journal of Computer Vision 60, 91-110 (2004)
27. Feng, J.: Combining minutiae descriptors for fingerprint matching. Pattern Recognition 41, 342-352 (2008)
28. Jain, A.K., Feng, J., Nagar, A., Nandakumar, K.: On matching latent fingerprints. In: Computer Vision and Pattern Recognition Workshops, 2008. CVPRW'08. IEEE Computer Society Conference on, pp. 1-8. IEEE
29. Jain, A., Hong, L., Bolle, R.: On-line fingerprint verification. Pattern Analysis and Machine Intelligence, IEEE Transactions on 19, 302-314 (1997)
30. Ballard, D.H.: Generalizing the Hough transform to detect arbitrary shapes. Pattern recognition 13, 111-122 (1981)
31. Kittler, J., Hatef, M., Duin, R.P., Matas, J.: On combining classifiers. Pattern Analysis and Machine Intelligence, IEEE Transactions on 20, 226-239 (1998)
32. Liu, E., Jain, A.K., Tian, J.: A coarse to fine minutiae-based latent palmprint matching. IEEE transactions on pattern analysis and machine intelligence 35, 2307-2322 (2013)
33. Tico, M., Kuosmanen, P.: Fingerprint matching using an orientation-based minutia descriptor. Pattern Analysis and Machine Intelligence, IEEE Transactions on 25, 1009-1014 (2003)
34. Cao, K., Liu, E., Pang, L., Liang, J., Tian, J.: Fingerprint matching by incorporating minutiae discriminability. In: Biometrics (IJCB), 2011 International Joint Conference on, pp. 1-6. IEEE
35. Hernández-Palancar, J., Muñoz-Briseño, A., Gago-Alonso, A.: A New Triangular Matching Approach for Latent Palmprint Identification. Progress in Pattern Recognition, Image Analysis, Computer Vision, and Applications, pp. 294-301. Springer (2013)

36. Gago-Alonso, A., Hernández-Palancar, J., Rodríguez-Reina, E., Muñoz-Briseño, A.: Indexing and retrieving in fingerprint databases under structural distortions. Expert Systems with Applications 40, 2858-2871 (2013)
37. Chikkerur, S., Cartwright, A.N., Govindaraju, V.: K-plet and coupled BFS: a graph based fingerprint representation and matching algorithm. Advances in Biometrics, pp. 309-315. Springer (2005)
38. Burrus, C.S., Gopinath, R.A., Guo, H., Odegard, J.E., Selesnick, I.W.: Introduction to wavelets and wavelet transforms: a primer. Prentice Hall, New Jersey (1998)
39. Fischler, M.A., Bolles, R.C.: Random sample consensus: a paradigm for model fitting with applications to image analysis and automated cartography. Communications of the ACM 24, 381-395 (1981)
40. Smith, R.: Inc.,“Demystifying palm prints,” http://www.ronsmithandassociates.com/. (2012)
41. Cappelli, R., Ferrara, M., Maio, D.: A fast and accurate palmprint recognition system based on minutiae. Systems, Man, and Cybernetics, Part B: Cybernetics, IEEE Transactions on 42, 956-962 (2012)
42. Cappelli, R., Ferrara, M., Maltoni, D.: Minutia cylinder-code: A new representation and matching technique for fingerprint recognition. Pattern Analysis and Machine Intelligence, IEEE Transactions on 32, 2128-2141 (2010)

RT_069, febrero 2015
Aprobado por el Consejo Científico CENATAV

Editor: Lic. Lucía González Bayona
Diseño de Portada: Di. Alejandro Pérez Abraham
RNPS No. 2142
ISSN 2072-6287
Indicaciones para los Autores:
Seguir la plantilla que aparece en www.cenatav.co.cu
CENATAV
7ma. A No. 21406 e/214 y 216, Rpto. Siboney, Playa;
La Habana. Cuba. C.P. 12200
Impreso en Cuba